5
Flexible RRAM Devices with in MoS_2:PVK/TiO_2 Hybrid Bilayer

In this chapter, PVK:MoS_2/TiO_2 hybrid bilayer exhibited excellent switching with low V_{SET} and V_{RESET} of 1.2 V and -1.5 V respectively, high endurance of 1000 cycles, and high stability upon bending with radii up to 7 mm for 100 cycles. These results are published in the [Saini et al., 2023]. A comprehensive investigation of long-term environmental stability and performance was also performed by systematically characterizing the devices for a duration of 20 months and it was found that devices were able to maintain their switching behavior with excellent retention of 10^4 seconds even after being in ambient environment for this long duration, indicating high shelf life. Moreover, effect of exposure to humidity and heating were studied confirming good stability against these. These investigations indicated suitability of PVK:MoS_2/TiO_2 as a switching layer candidate for environmentally stable RRAM devices for flexible electronics. These results are recently published [Saini et al., 2024].

5.1 Introduction

Flexible electronics as an emerging field has garnered significant attention due to its versatility and potential applications in flexible touch sensors, rollable display screen, on-body wearables and implantable devices for health monitoring, and so forth [Abbas et al., 2023, Wang et al., 2020, Gao et al., 2019]. Flexible electronic devices are expected to be capable of withstanding not only bending and folding but also compression and stretching without any significant change in their electrical properties [Liu et al., 2022]. For progress of any technology, suitable nonvolatile memory devices are essential. Various next-generation emerging nonvolatile memory candidates, such as ferromagnetic RAM (FeRAM), magnetic random access memory (MRAM), phase change memory (PCM), and resistive random access memory (RRAM), have been explored in the last decade due to their high-performance capabilities and simple structures [Fong et al., 2017, Bhatti et al., 2017, Ishiwara, 2012, Pan et al., 2014]. Among these, RRAM devices have emerged as the front runner due to excellent capabilities such as rapid switching speed, low power consumption, CMOS compatibility, ease of fabrication, and 3-D stacking possibility [Wong et al., 2012] [Luo et al., 2016, Choi et al., 2016, Lodhi et al., 2022]. With the advent of flexible electronics against the backdrop of the current technological paradigm, hybrid dielectric layered RRAMs have attracted significant attention due to their high reliability, low-power switching operation, and high I_{ON}/I_{OFF}, making them a key memory candidate for flexible electronics [Varun et al., 2020, Nagareddy et al., 2017]. The term "hybrid" refers to an unconventional layered structure containing organic polymers or polymer composites and inorganic dielectrics or both. To be integrated in flexible electronics systems, high values of retention time, endurance, and I_{ON}/I_{OFF} along with mechanical stability and low-voltage operation are desired [Wu et al., 2019, An et al., 2020, Aziz et al., 2021]. hybrid RRAMs—inorganic materials such as HfO_x, TiO_x, and AlO_x [Lee and Cho, 2017, Kim et al., 2010, Yuan et al., 2014, Maikap and Banerjee, 2020]; organic polymers such as Polymethyl methacrylate (PMMA), poly(4-vinylphenol) (PVP), poly(N-vinylcarbazole) (PVK), and polyvinyl alcohol (PVA) [Yang et al., 2017, Kim and Hwang, 2021, Li et al., 2018, Rehman et al., 2016]; and low-dimensional materials such as molybdenum disulfide (MoS_2), boron nitride (BN), tungsten disulfide (WS_2), and others [Bhattacharjee et al., 2017, Sun et al., 2021, Lee et al., 2019]. MoS_2 is one of the most widely studied candidates of transition metal dichalcogenides in the family of 2-D materials. In last few years, MoS_2 has attracted lot of attention as a promising resistive switching material for RRAM devices due to its atomically thin nature, favorable chemical and thermal stability, electron affinity (EA~3.74–4.45 eV), thermal conductivity (16.2 W/mK), good dielectric constant (4–17), and higher mobility of cations

compared to the other metal oxides [Ginnaram and Maikap, 2021, Ginnaram et al., 2020, Dutta et al., 2020]. Composites of MoS_2 and polymeric dielectric materials have been explored in RRAM devices due to their ability to enhance the suitability for bending, high carrier mobility, low power consumption, and intrinsic flexibility [Varun et al., 2020, Zhang et al., 2016]. Preparing composite may need high loadings of MoS_2; however, at high loadings, issues, such as phase separation, occur due to noncovalent modification of MoS_2 with polymers, which have been addressed by using active layers of MoS_2 covalently modified with polymer by techniques such as liquid exfoliation [Zhang et al., 2016]. Using MoS_2 with polymers, operations, such as rewritable memory and write once read many memories, are reported due to structural phase transition, for example, with MoS_2-PVP on flexible PET substrate by [Zhang et al., 2016], PVK, a thermoplastic polymer that has temperature resistance, wide bandgap, charge storage, and excellent film formation properties [Ling et al., 2017] can be a preferable candidate for flexible and printable memory devices [Li et al., 2018]. Though already reported in rigid RRAMs [Fan et al., 2017, Lai and Chen, 2009, Zhang et al., 2018], PVK is still unexplored in combination with MoS_2 for flexible RRAMs. Moreover, TiO_2, which is a promising oxide material explored in flexible RRAMs through various strategies [Kim et al., 2021, Pham et al., 2016, Zhao et al., 2018], can be an excellent candidate to be studied with of PVK:MoS_2 composite. TiO_2 has shown the capability to demonstrate both unipolar resistive switching and bipolar resistive switching [Pham et al., 2016, Irshad et al., 2019], high thermal stability [Promjun et al., 2022], and wide bandgap (3–3.2 eV), which results in low leakage current in the HRS in the fabricated devices. The atomic layer deposition (ALD) technique is used in the deposition of thin TiO_2 film, providing various advantages of high-quality films, uniformity, low processing temperature, and device reliability [Jeong et al., 2010]. In the fabricated PVK:MoS_2/TiO_2/ITO RRAM device, MoS_2 plays a crucial role as a charge trapping centre and a conductive pathway modulator within the PVK. The layered structure of MoS_2 provides abundant defect sites, edge states, and sulfur vacancies that facilitate charge trapping and influence filament formation during the resistive switching process [Varun et al., 2020, Zhang et al., 2016]. MoS_2 enhances the composite's dielectric properties when embedded in PVK, leading to stabilization of the switching mechanism. It contributes to improved I_{ON}/I_{OFF} and retention stability by enabling controlled filament growth and rupture.

Although these devices exhibited excellent switching, endurance, and flexibility, crucial performance aspects, such as operational stability upon exposure to varying environmental conditions, such as humidity and temperature and shelf life, are essential to be investigated for realistic applications. Shelf life is a measure of time duration for which the device maintains its operation when kept or stored in normal ambient. It is also referred as long-term environmental stability. The environmental stability of flexible RRAM devices is a major concern as the materials utilized in fabrication have performance limitations depending on the operating environment, for example, the devices fabricated on flexible substrate PET cannot be utilized above 100 °C as PET starts distorting after 100 °C and PEN substrate after 150 °C [Boehme and Charton, 2005, Serrano et al., 2020]. Similarly, an organic material degrades with time. Similar limitations are based on humidity, moisture, and other environmental condition [Iqbal et al., 2021, Yun and Choi, 2019]. Thus, the investigation of shelf life and environmental stability is essential for RRAM devices [Sun et al., 2023]. Both of these requirements, which are high shelf life and high stability in ambient, are important for commercialization of products based on these devices. Although reports on high-performance flexible RRAM devices can be found in literature, the reports on comprehensive investigation of shelf life and stability of flexible RRAM devices are scarce.

5.2 Fabrication of Ag/MoS_2:PVK/TiO_2/ITO Flexible RRAMs

RRAM devices were fabricated on flexible and transparent PEN substrate coated with ITO, which acts as BE. Cleaning of PEN substrate was done using an ultrasonic bath in methanol and isopropyl alcohol followed by drying with N_2 blow. TiO_2 of thickness 10 nm was deposited over ITO at 150 °C using Savannah S200 thermal ALD system using tetrakis(dimethylamido)titanium (IV) and deionized water as precursors: Poly (9-vinylcarbazole) (PVK) (MW = 1100000) and MoS_2

(MW=160.07g/mol). The substrates and materials used for device fabrication were procured from Sigma-Aldrich. A 2 wt% PVK solution was prepared in chlorobenzene solvent and spin coated over TiO_2 at 2000 r/min for 45 seconds. The PVK:MoS_2 composite solution was prepared by the organic polymer liquid exfoliation method [Zhang et al., 2016]. For the same, first, 200 mg of PVK and 50 mg of MoS_2 were added to 10-mL chlorobenzene. The mixture was ultra-sonicated for 12 hours yielding to a dark green color suspension, which was further kept in a vacuum for 72 hours for settling down of undesired heavy particles. The upper part (80%) of the solution was centrifuged at 6000 r/min for half an hour providing a greenish-yellow super natant, which contains MoS_2 nanoparticles bonded through PVK polymer in chlorobenzene solvent. This supernatant solution was spin coated over TiO_2 at 2000 r/min for 45 seconds to form a ~80-nm-thick film of PVK:MoS_2. Samples were annealed on the hotplate at 90 °C for 1 hour to remove the residual solvent. Finally, using thermal evaporation under the high vacuum of 1.5×10^{-6} torr, ~200-nm-thick circular Ag TE with a 400 µm diameter were deposited using shadow mask. Keithley 4200 SCS was used for the electrical characterization of the devices. AFM of SPM XE-70 from Park Systems was used to capture surface morphologies of fabricated devices. Reference devices were also fabricated with neat PVK over TiO_2 only for comparison. The schematic and digital image of fabricated device is shown in Figure 5.1(a & b). Chemical structure of MoS_2 and PVK are shown in Figure 5.1(c & d) respectively.

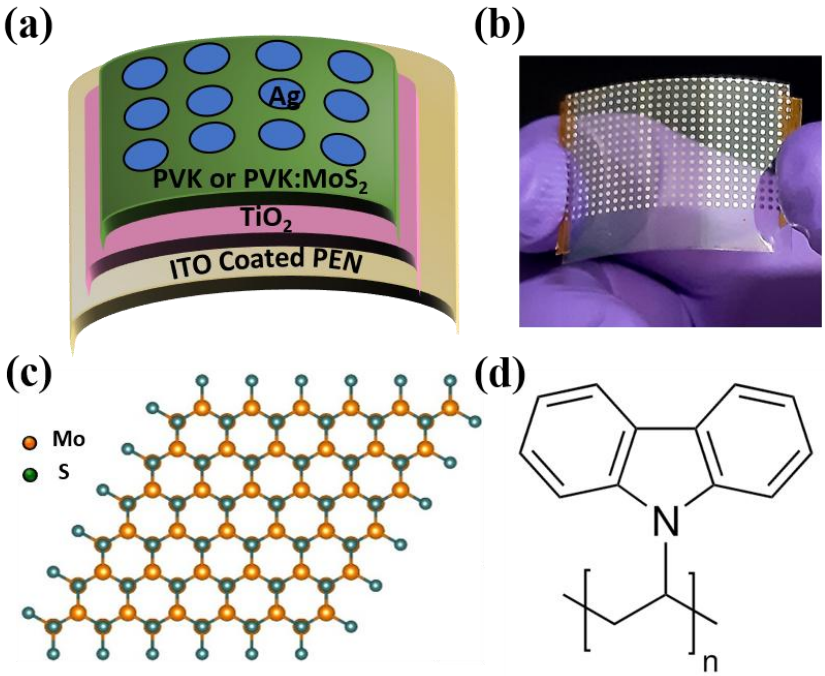


Figure 5.1 Schematic structure **(a)** and digital picture **(b)** of fabricated flexible RRAM device. AFM image of PVK/TiO2 film **(c),** and PVK:MoS_2/TiO_2 film **(d).**

Furthermore, to study the effect of exposure to additional RH values on switching performance, the devices were exposed to various humidity levels (RH~42% to ~99%), and the corresponding variation in electrical characteristics was investigated. Moreover, for investigating the effect of temperature, devices were heated for 1 hour on a hot plate right before the electrical characterization for the temperatures of 50 °C, 80 °C, and 100 °C. To support these findings, the effect of temperature on properties of PVK, MoS_2 and their composite (PVK:MoS_2) and their thermal stability were analyzed by thermogravimetric analysis (TGA) with Perkin Elmor STA 6000 and through differential scanning calorimetry (DSC) by Perkin Elmor DSC 4200 system.

5.3 Results and Discussion

5.3.1 Film and Material Characterization

Figure 5.2(a), shows the UV–visible spectroscopy plot of MoS_2. The highest absorbance of UV light in MoS_2 was found at a wave length of 596 nm. The corresponding energy versus $(ahv)^2$ plot also known as Tauc plot is presented in Figure 5.2(b), where a indicates the absorption coefficient, h is Planck's constant, and schematic and v is the intensity of light. The Tauc plot is used to measure the energy bandgap (E_g) through the intercept of linear fit at maximum slope of the plot at the X-axis, as shown in Figure 5.2(b). E_g of MoS_2 was found to be ~1.9 eV through this plot, which also matches with earlier reports [Peng et al., 2016]. To understand the variations in the performance of flexible RRAM devices after heating at various temperatures, the thermal properties of PVK:MoS_2 were investigated in detail through TGA and DSC techniques. Along with PVK:MoS_2, these measurements were also performed on pristine PVK and MoS_2 to understand the variations in the material properties from pristine materials to composite. Although these measurements were also done for much higher temperatures, the changes occurring below 100 °C were given more attention. It is important to note that glass transition temperature of PEN is about 122 °C and the substrates deform at about 150 °C [Serrano et al., 2020]. One other potential substrate, PET, has a glass transition temperature of 78 °C, with observable deformation at about 100 °C [Zhang et al., 2004]. The TGA and DSC plots for pristine MoS_2, PVK, and PVK:MoS_2 composite are shown in Figure 5.2(c & d), respectively. These characteristics help in comparing the thermal stability of these materials. As highlighted in the inset of Figure 5.2(c), the weight loss observed from PVK:MoS_2 composite is in between the pristine materials up to about 115 °C. At 100 °C, PVK:MoS_2 composite exhibited very high thermal stability with a negligible weight loss of only 0.37%, which is suitable for devices on flexible substrates. DSC results also support these findings with negligible changes in heat flow with increasing temperature in the region of interest.

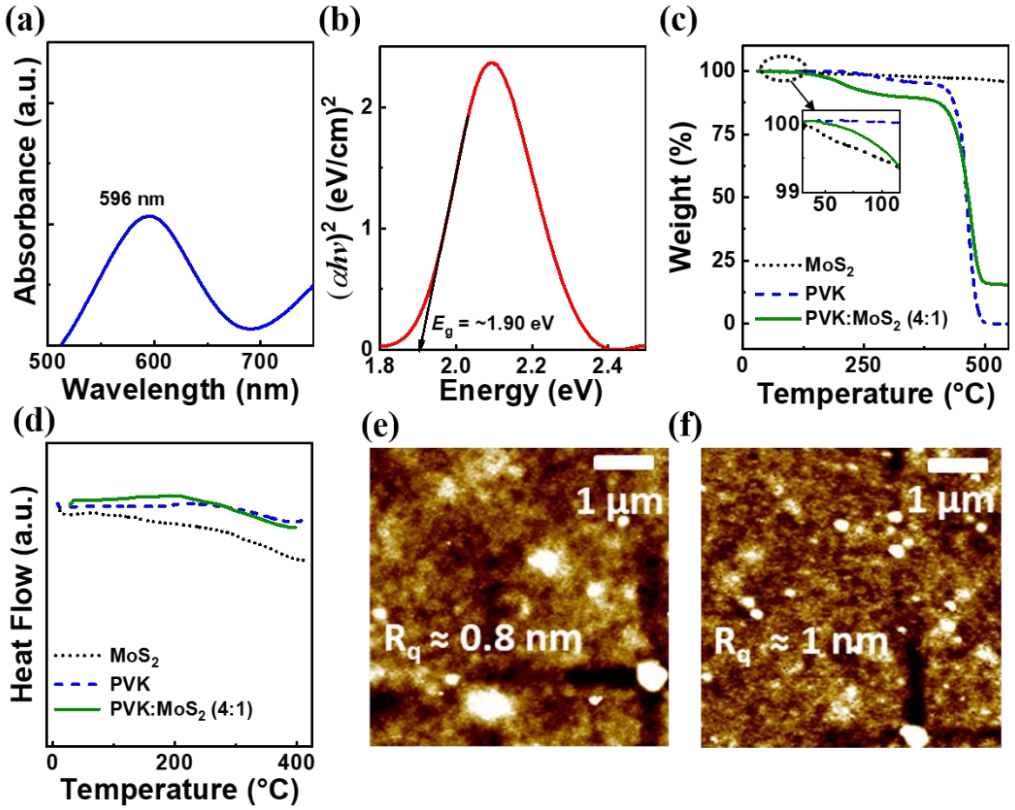


Figure 5.2 UV-Visible absorbance spectroscopy **(a)** and Tauc plot **(b)** of MoS_2. Plots of TGA **(c)** and DSC **(d)** for PVK, MoS_2, and PVK:MoS_2 composite. AFM image of surface of PVK/TiO_2 **(e)** and PVK: MoS_2/TiO_2 **(f)**.

Figure 5.2(e & f) show the AFM images of surface of neat PVK and PVK:MoS_2 thin films deposited over TiO_2, respectively. The root-mean-square (rms) roughness values of top surface of neat PVK and PVK:MoS_2 thin films over TiO_2 were obtained to be ~0.8 and ~1.0 nm,

respectively, indicating extremely smooth surfaces for both cases. The difference in roughness is less than 0.2 nm, which may be attributed to the presence of a 2D MoS_2 material.

5.3.2 Electrical Performance of Flexible RRAMs

Devices were characterized for electrical performance by applying the continuous voltage sweep from 0 → V_{max} → 0 → $-V_{max}$ → 0 across the TE and BE. A compliance current of 1 mA was applied on positive cycle to prevent the device from permanent failure. The *I–V* characteristics of formation cycle in neat PVK/TiO_2 and PVK:MoS_2/TiO_2 are given in Figure 5.3(a) & (b), respectively. Both these devices exhibit bipolar switching behavior; however, neat PVK/TiO_2 devices required a higher voltage application of −3 → 0 → 3 V for switching operation and switched at the SET voltage of 2 V and the RESET voltage of -1 V. On the other side, PVK:MoS_2/TiO_2 devices operated at lower voltages. A DC voltage sweep of 0 → 1.5 V was applied and a sharp change in current was observed at the SET voltage of 1.2 V. Changes from HRS to LRS can be observed from these results indicating conducting filament formation between TE and BE of the device. Furthermore, 0 to −1.8 V negative voltage sweep was applied to the device and a sharp change in current was observed at −1.5 V RESET voltage. The device reached HRS from LRS due to the process of filament rupture.

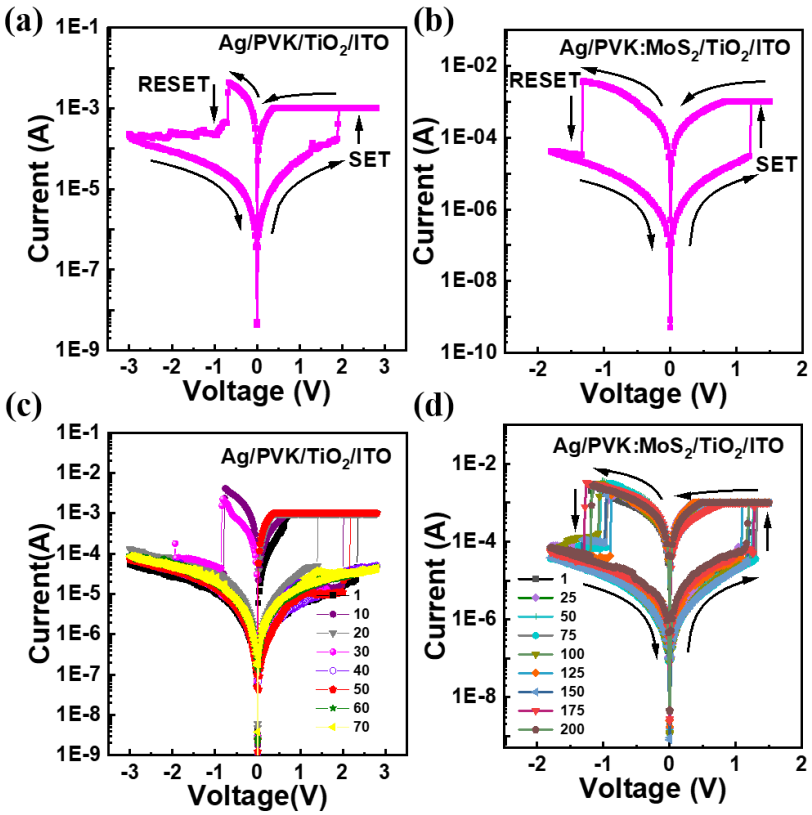


Figure 5.3 (a) *I–V* characteristics and **(c)** multiple cycles of Ag/PVK/TiO_2/ITO. **(b)** *I–V* characteristics and **(d)** multiple cycles of Ag/PVK:MoS_2/TiO_2/ITO.

Figure 5.3(c) shows the repeatability plot for Ag/PVK/TiO_2/ITO devices up to 70 cycles. As it can be seen, the device is not SET for most of the cycles. On the other hand, Ag/PVK:MoS_2/TiO_2/ITO RRAM devices exhibited excellent repeatability, as shown in Figure 5.3(d). No remarkable degradation in the memory window was observed during repeatability for 200 cycles. The corresponding endurance plots for both devices at a read voltage of 0.2 V are shown in Figure 5.4(a & b). In addition, the retention characteristics of the first cycle for 5000 s are shown in 5.4(c & d). As it can be seen, endurance for Ag/PVK:MoS_2/TiO_2/ITO device is significantly better than the reference (Ag/PVK/TiO_2/ITO) device, which does not reach its LRS state on most of the instances, indicating poor endurance. On the other hand,

Ag/PVK:MoS_2/TiO_2/ITO devices exhibited a decent I_{ON}/I_{OFF} of more than 10^2 during the 200 cycles, as shown in Figure 5.4(b). A slight decrease in both LRS and HRS is seen with an increasing number of cycles for this device, which corresponds to slight variations observed in repeatability plots. This decrease may be attributed to the random movement of ions during the switching process [Pan et al., 2014]. The decrease in HRS can also be attributed to the increasing filament dissolution strength [Wong et al., 2012], which is due to increasing RESET voltage, as shown in Figure 5.4(d). Moreover, the variation in LRS is random, as explained earlier [Wong et al., 2012]. Further exploration for these issues may be needed for better understanding. Though the retention time plot of Ag/PVK/TiO_2/ITO for the first cycle shows a high I_{ON}/I_{OFF}, these devices did not reach in SET state after few cycles. To emphasize, the Ag/PVK:MoS_2/TiO_2/ITO devices maintained the resistive switching for all the investigated cycles with excellent stability. A decent I_{ON}/I_{OFF} of more than 10^2 was maintained, confirming the nonvolatile property.

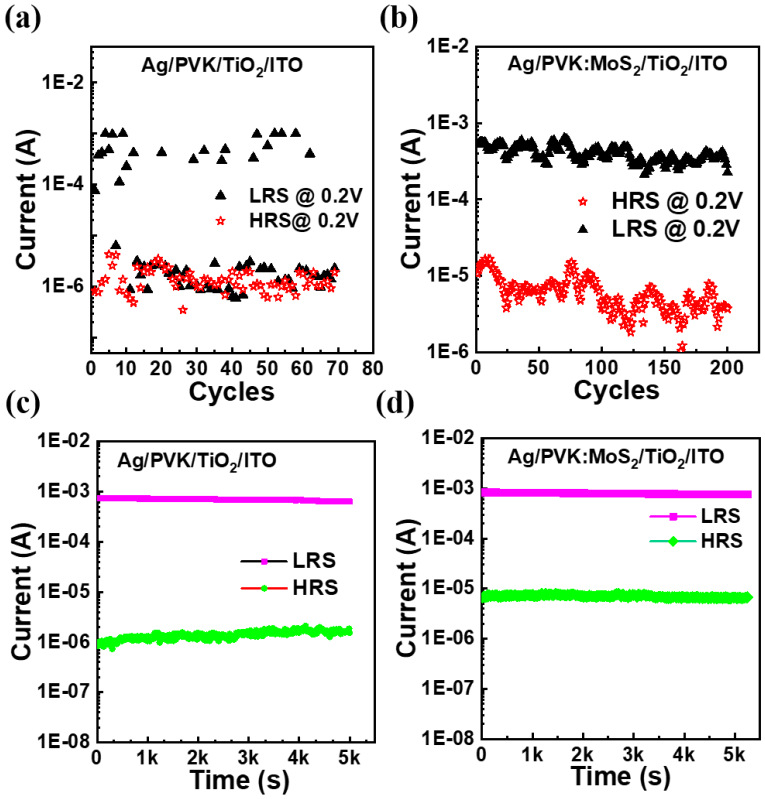


Figure 5.4 Endurance characteristics at 0.2-V read voltage of devices: **(a)** Ag/PVK/TiO_2/ITO and **(b)**Ag/PVK: MoS_2/TiO_2/ITO. **(c) & (d)**Retention characteristics of Ag/PVK/TiO_2/ITO and Ag/PVK:MoS_2/TiO_2/ITO devices, respectively. Both the LRS and HRS currents are taken at 0.2 V read voltage.

5.3.3 Conduction & Switching Mechanism

The conduction mechanism for both devices was investigated using double log I–V plots, as shown in Figure 5.5. The SET process for Ag/PVK:MoS_2/TiO_2/ITO device is shown in Figure 5.5(a). It shows a slope value of ~1.2 in low voltage, i.e., ohmic region of the device indicating ohmic conduction due to partially filled trap sites and thermally generated charge carriers. When the applied voltage further increases, the slope of the log (V) versus log (I) graph reaches a maximum of ~1.5. It indicates that inside the dielectric layer, all trap sites are filled. The steep current switching follows the SCLC, which is governed by Child's law. The space charge has entirely regulated the current in this region, preventing any further charge carrier injection. Furthermore, the sharp rise in current indicates that the device has reached the SET state and a metallic filament has been formed. When voltage decreases in the SET region, the current decreases linearly, which is indicated by a slope value of ~1 and indicates ohmic conduction. Similarly, in the RESET state, as shown in Figure 5.5(b), initially, a conducting filament is present, and thus, a slope value of ~1 is obtained. At higher voltage when the filament rupture starts, the

double log *I–V* characteristic follows Child's law with a slope value of ~1.7. After the filament dissolution, at a lower voltage, ohmic conduction (slope ~1) is observed. The conduction mechanism of Ag/PVK/TiO_2/ITO device is shown in Figure 5.6(c) for SET and Figure 5.5(d) for RESET. In this case also, at lower voltage, ohmic conduction is indicated (slopes value of ~1 and ~1.2), whereas the SCLC mechanism is dominant at higher voltages (slopes of ~1.8 and ~1.4). Devices with PVK:MoS_2/TiO_2 switching layer were further investigated for reliability and performance.

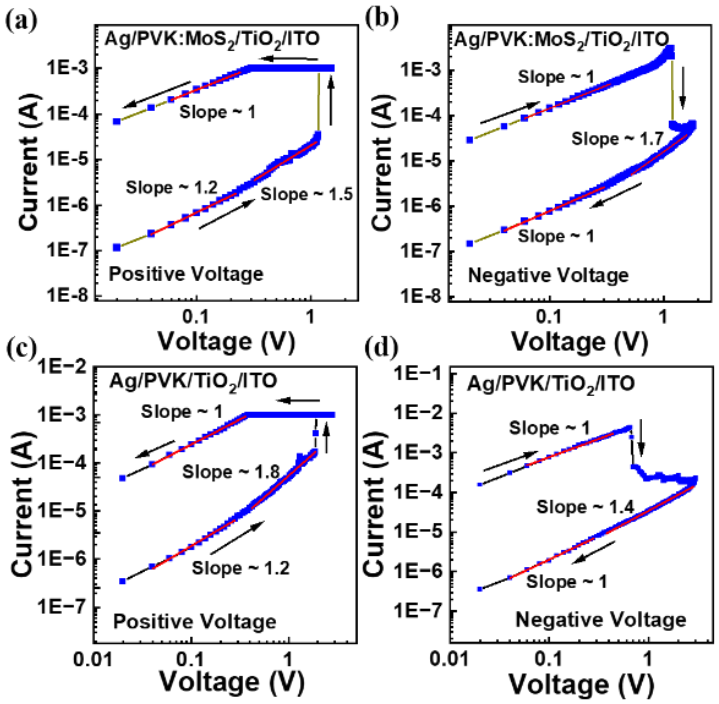


Figure 5. 5 Double log *I–V* characteristics of Ag/PVK:MoS_2/TiO_2/ITO **(a)** & **(b),** and Ag/PVK/TiO_2/ITO **(c)** &**(d)** for positive and negative voltage sweep.

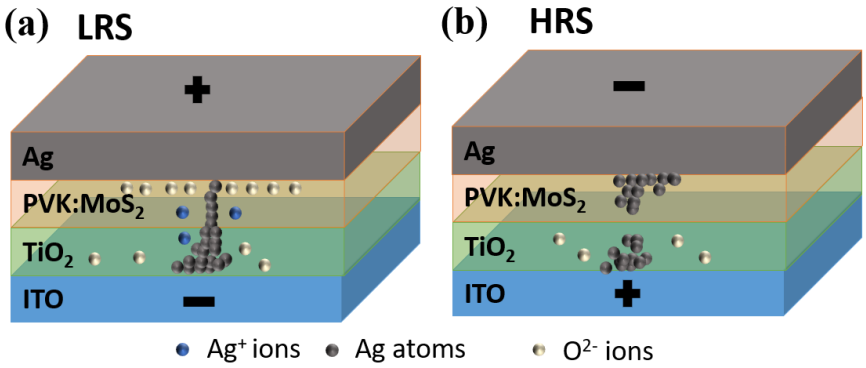


Figure 5.6 Schematic of the switching mechanism for **(a)** LRS and **(b)** HRS showing the movement of Ag and oxygen ions.

Given the preceding description and switching properties under various test situations, it appears that the filament-type switching mechanism occurs in these devices. The formation and rupture of many weak Ag filament by electromigration of Ag atoms between TE and BE switch the device from HRS to LRS and vice versa, as shown schematically in Figure 5.6(a & b). Ag atoms from TE oxidize to Ag^+ ions upon application of positive voltage sweep (0 → 1.5 V) to the TE, i.e., active metal contact. These ions then migrate toward the BE under the influence of the electric field. Upon reaching the BE, Ag^+ ions get reduced to Ag atoms followed by accumulation of Ag atoms at BE. This continuous process will eventually lead to the formation of conducting filament

between BE and TE, as shown in Figure 5.6(a). At this point, a spike in current will be noticed at V_{SET} and the device will be switched to LRS from HRS, which is referred to as WRITE operation or SET procedure. The creation of many weak nano-sized Ag filaments in the switching layer can help in low-voltage or low-current switching [Zhang et al., 2016, Hua et al., 2019]. The LRS of the device was maintained when the potential was swept back from 1.5 to 0 V, which indicates nonvolatile memory behavior. Now, to erase the data or change the state from LRS to HRS, a negative voltage sweep is applied across the electrodes. Upon application of negative bias, specifically at V_{RESET}, the weak filaments rupture or break causing a sharp decrease in current and Ag^+ ions will drift back to the TE. This switches the device back to HRS and is referred to as RESET processes, as shown in Figure 5.6(b), and it is previously described using the Gibbs–Thomson effect, in which filaments based on electrochemically active metals such as Ag or Cu help in switching performance of the device [Hua et al., 2019, Zhang et al., 2016, Shen et al., 2020].

5.3.4 Bending Stability

Furthermore, the variation of performance upon bending of these devices was investigated, as shown in Figure 5.7. Figure 5.7(a) shows the switching characteristics of a particular device at the unbent condition and with different bending radii, showing a reliable switching performance while maintaining the current ratio of $\geq 10^2$ until 10 mm of bending. Figure 5.7(b), shows the corresponding retention curves for a read voltage of 0.2 V for 5000 s showing excellent data retention properties for extreme bending conditions.

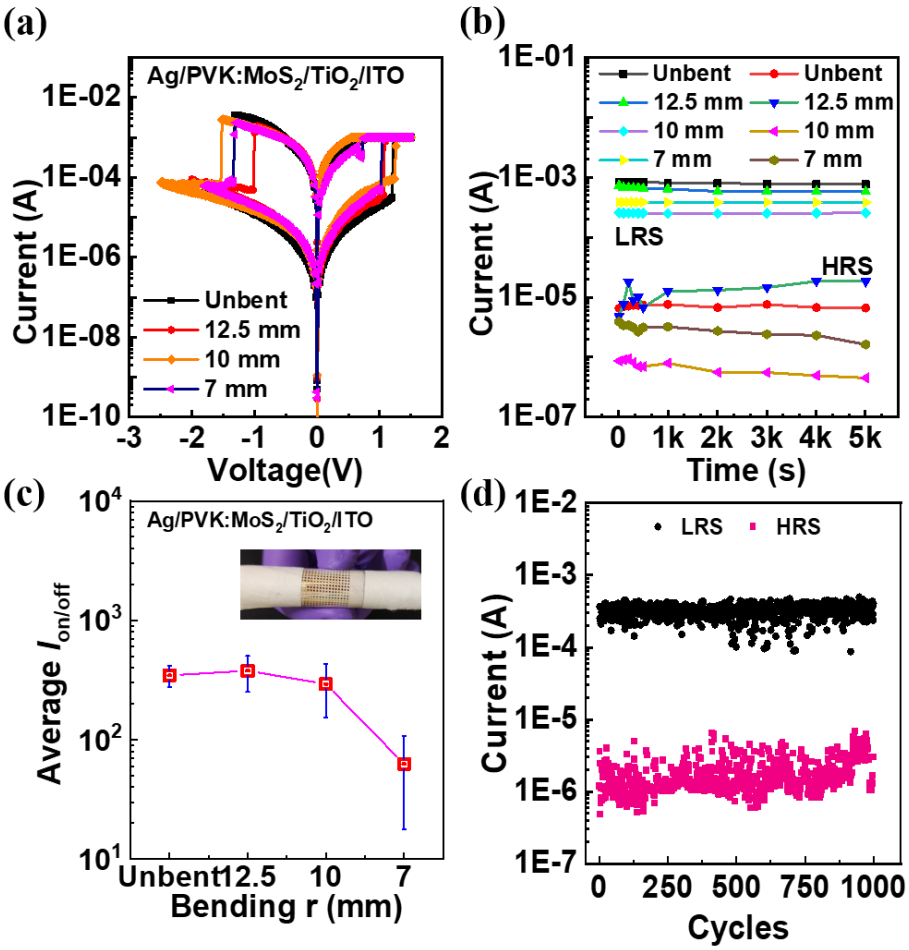


Figure 5.7 (a) *I–V* characteristics for unbent, 12.5, 10, and 7 mm bending. **(b)** Retention time analysis for unbent and bent conditions for 5000 s at 0.2-V read voltage for HRS and LRS current. **(c)** Standard deviation and average I_{ON}/I_{OFF} of device with and without bending. Inset shows the digital image of the bent device. **(d)** Endurance characteristics for 1000 cycles at 0.2 V read voltage, after bending studies and aging for two months.

Figure 5.7(c) shows the average switching I_{ON}/I_{OFF} for more than ten devices at each bending radius. As it can be observed, switching I_{ON}/I_{OFF} ~300 is maintained until 10 mm of bending. Upon further bending at being radius of 7 mm, it deteriorates to less than 100, as expected for extreme bending conditions due to possible microcracks inside the films. The digital image of a bent device is shown in the inset of Figure 5.7(c). Figure 5.7(d), shows the endurance of the device for 1000 cycles with a read voltage of 0.2 V, after the bending studies and aging for about two months. This endurance study shows that the device is able to maintain its resistance states even after 1000 cycles operations.

5.3.5 Shelf-Life Stability

A comprehensive investigation of long-term environmental stability and performance of flexible hybrid RRAM devices with PVK:MoS_2/TiO_2 bilayer is presented. These devices were systematically characterized for their switching behavior for a very long duration of 20 months. The switching characteristics of a particular flexible RRAM device with PVK:MoS_2/TiO_2 hybrid switching layer plotted for pristine as well as for time instances of 3, 6, 10, 11, 12, and 20 months after fabrication are shown in Figure 5.8(a).

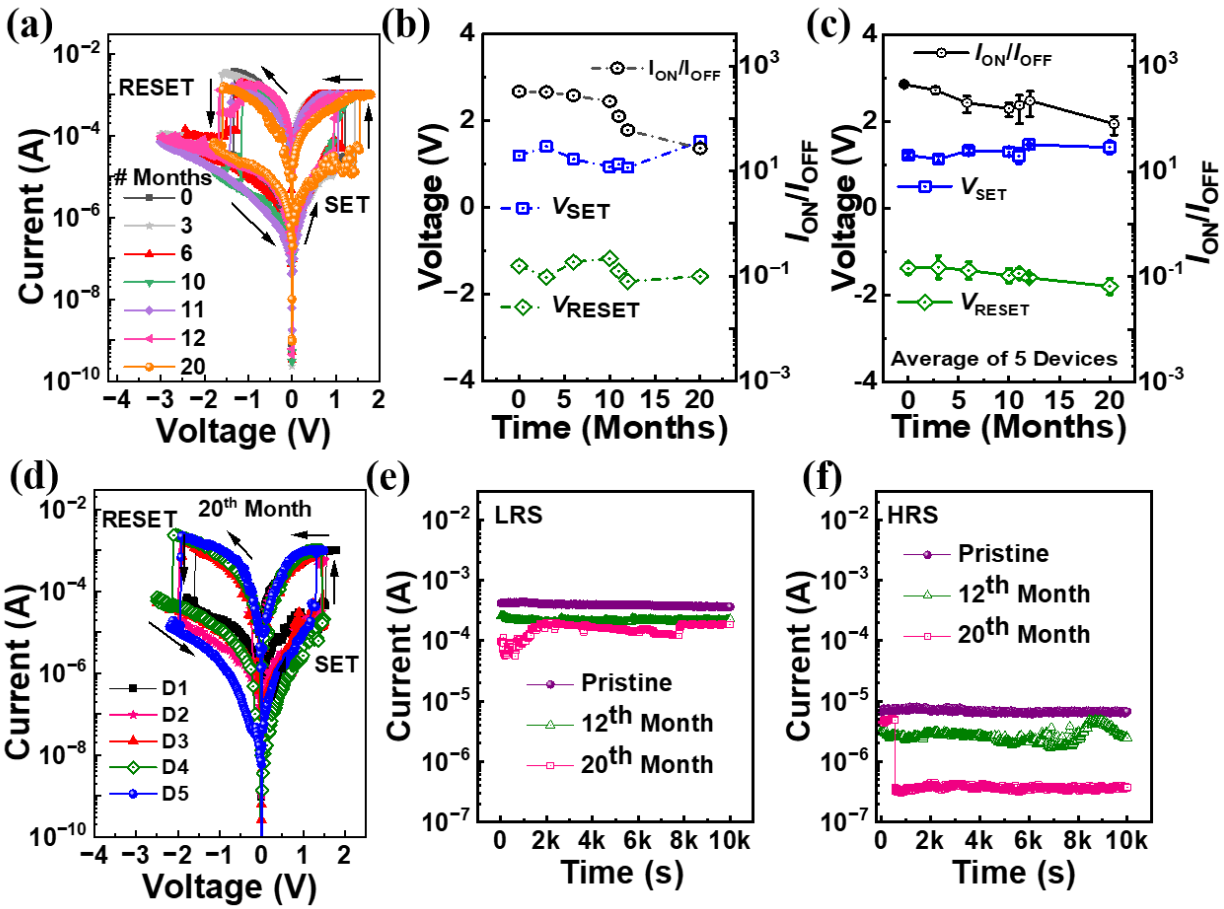


Figure 5.8 Plots of switching characteristics **(a)** and corresponding V_{SET} and V_{RESET} and I_{ON}/I_{OFF} **(b)** of a particular device. **(c)** Plots of average values of V_{SET} and V_{RESET} and I_{ON}/I_{OFF} of five devices on a substrate investigated after 3, 6, 10, 11, 12, and 20 months. **(d)** *I-V* characteristics of five devices on a substrate after 20 months, indicating excellent shelf life. Retention characteristics of pristine, 12th month, and 20th month of characterization for **(e)** LRS and **(f)** HRS.

For the same, the *I-V* characteristics were measured by applying a DC voltage sweep (0→ 1.8 V → 0 → −3 V → 0) across the TE and BE. A compliance current of 1 mA was applied for positive cycle side only to reduce the chance of damaging the device with high current. Excellent and consistent resistive switching can be observed from these *I-V* characteristics. The variation in V_{SET}, V_{RESET}, and I_{ON}/I_{OFF} of this particular device at various time instances is depicted in Figure

5.8(b). It was found that the I_{ON}/I_{OFF} was almost unchanged for up to initial 10 months. A degradation was seen for more than an order of magnitude after 20 months; however, the switching behavior was still intact with distinct LRS and HRS states. Minimal variations in the extracted values of V_{SET} and V_{RESET} of this device were observed during 20 months, from ~1.2 to ~1.5 V and -1.3 to -1.6 V, respectively, exhibiting high reliability of switching. To get the statistical data, five devices of a substrate were characterized for all the time instances, i.e., after 3, 6, 10, 11, 12, and 20 months. Moreover, the plots of average values of V_{SET} and V_{RESET} with standard deviation are shown in Figure 5.8(c), along with corresponding average I_{ON}/I_{OFF} values for all time instances. The plots of *I-V* characteristics of those five devices on a substrate characterized after 20 months are shown in Figure 5.8(d), indicating acceptable device to device variation of switching performance. The average values of the extracted V_{SET} and V_{RESET} of these five devices of a substrate characterized for all time instances are summarized in Table 5.1. Average V_{SET} and V_{RESET}, respectively, varied between ~1.1 and 1.5 V and −1.0 and -1.8 V, again indicating high long-term stability in switching behavior of these flexible RRAM devices with PVK:MoS_2/TiO_2 hybrid bilayer.

Table 5.1 : Average V_{SET} And V_{RESET} of Five Flexible RRAM Devices with PVK:MOS_2/TIO_2 Hybrid Bilayer From a Substrate Characterized for 20 Months.

Months	**0**	***3***	***6***	***10***	***11***	**12**	**20**
V_{SET} (V)	1.22 (± 0.05)	1.13 (±0.08)	1.33 (±0.06)	1.30 (±0.10)	1.20 (±0.17)	1.46 (±0.02)	1.40 (±0.14)
V_{RESET} (V)	-1.38 (± 0.13)	-1.36 (±0.26)	-1.43 (±0.20)	-1.55 (±0.16)	-1.50 (±0.12)	-1.60 (±0.07)	-1.80 (±0.18)

These results also indicated low device to device variability, which is highly desirable. The RESET voltages reported for these devices (with average V_{RESET} varying from -1.0 to -1.8 V in 20 months) are a bit higher compared to the RESET voltages of many recently reported CBRAM devices with Ag TE and Ag metallic filament (~-0.5 to -1.2 V) [Bala et al., 2023, Chen et al., 2020, Ali et al., 2022]. It is important to note here that the operating voltages are dictated by the nature of the filament, and devices with active metal electrodes may also have oxygen vacancies participating in the filament formation process [Dwivedi et al., 2022, Varun et al., 2020, Saini et al., 2023]. The slightly higher RESET voltages reported in this work may be attributed to the presence of oxygen vacancies in the conductive filament of our devices. Although the metallic filament is expected to be formed, the contribution of oxygen vacancies in switching cannot be nullified due to the presence of TiO_2 in hybrid switching layer (TiO_2/MoS_2:PVK) used in our devices [Saini et al., 2023]. Moreover, these complex hybrid bilayers need more exploration for understanding the nature of the conductive filament. The plots of retention characteristics of LRS and HRS for 10^4 seconds at read voltage of 0.2 V are shown in Figure 5.8(e & f) respectively, for pristine, 12, and 20 months. As it can be seen from the results, though LRS is fairly stable, the HRS decreases significantly for an order of magnitude due to the effect of aging.

5.3.6 Humidity and Temperature stability

Figure 5.9 summarizes the investigations of variation in resistive switching performance upon exposure to high humidity levels. For the systematic investigation of performance upon humidity exposure, devices were kept in humidity chamber for 1 hour at each level (RH% of 42, 84, and 99) right before characterization. The *I-V* characteristics for each RH% and after 24 hours in ambient are shown in Figure 5.9(a). The plots of average values of V_{SET}, V_{RESET}, and I_{ON}/I_{OFF} of five devices at each RH% are shown in Figure 5.9(b).

It can be clearly seen from Figure 5.9(b), that the I_{ON}/I_{OFF} slightly increases upon initial increase in humidity exposure. This increase in I_{ON}/I_{OFF} was seen to be maintained by the device after 24 hours of humidity exposure. The values of V_{SET} and V_{RESET} were fairly stable throughout the exposure range with acceptable magnitude of variation of ~0.3 and ~0.75 V, respectively. The

devices were further tested for temperature stability. Figure 5.10 summarizes the results for the investigation of performance variation upon heating at temperatures varying from room temperature (RT) to 100 °C for 1 hour before characterized.

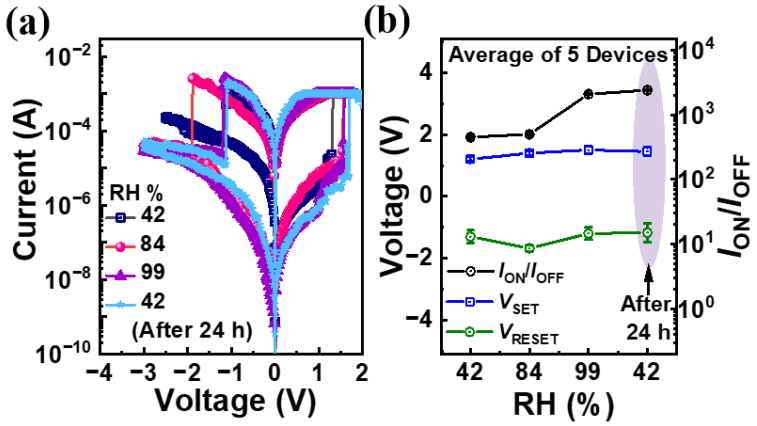


Figure 5.9 (a) Plots of *I-V* characteristics of a particular device upon exposure to different RH% levels (42, 84, 99, and after 24 hours at 42 %) and **(b)** corresponding plots of average values of V_{SET} and V_{RESET} and I_{ON}/I_{OFF} of five devices upon humidity exposure.

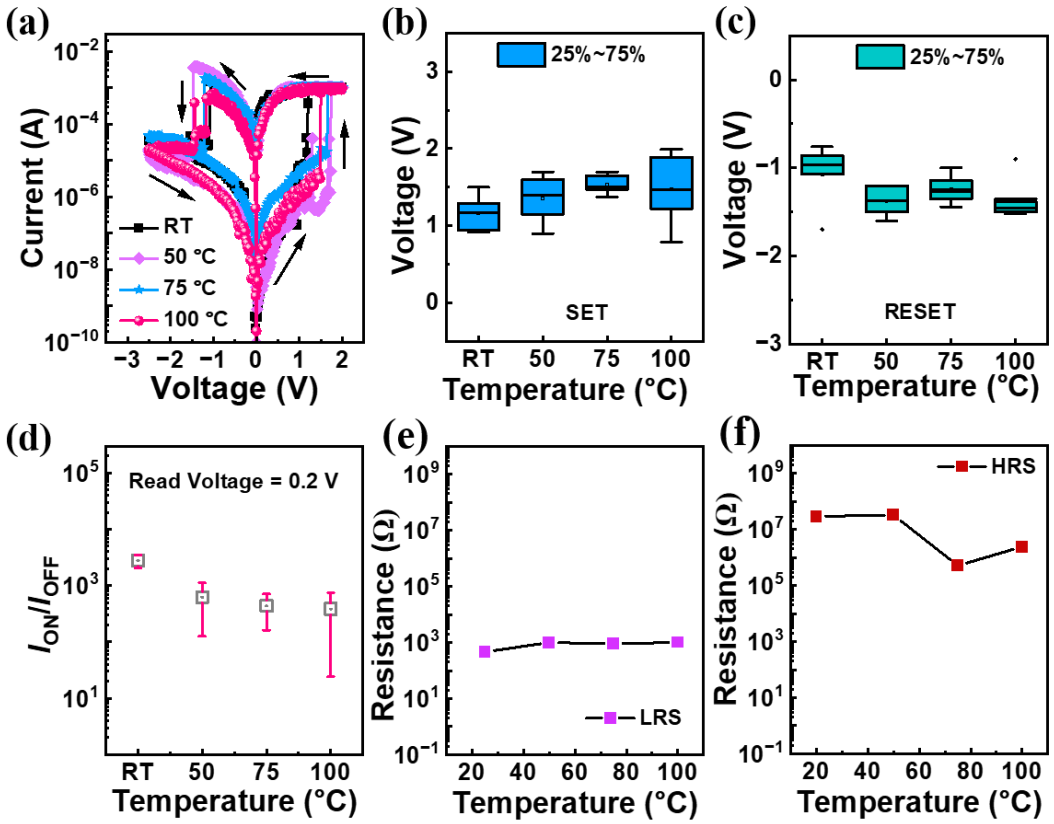


Figure 5.10 Variation of switching performance with heating temperature variation from RT to 100 °C. **(a)** *I-V* characteristics, Distribution of SET **(b)** and RESET voltage **(c),** and average I_{ON}/I_{OFF} for ten cycles **(d). (e)** Plots of LRS and **(f)** HRS at various heating temperature values.

The variation in V_{SET} and V_{RESET} with increasing heating temperatures is shown in Figure 5.10(b & c) respectively. It can be observed that the magnitudes of required SET and RESET voltages have slightly increased with the increase in temperatures. The average I_{ON}/I_{OFF} for ten cycles of measurements and standard deviation with variation of temperature are plotted in Figure 5.10(d). The average I_{ON}/I_{OFF} decreases with the increase in temperature from RT to 100

°C from ~3 × 10^3 to ~4 × 10^2. As it can be seen, though the devices show the excellent switching performance at RT, a decay in performance is observed for 1 hour heating at 100 °C.

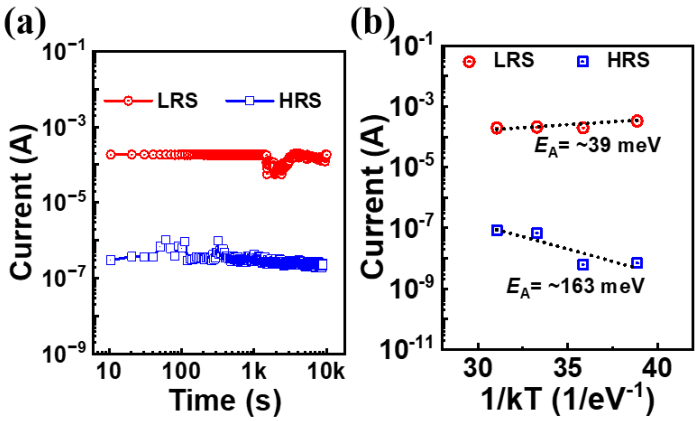


Figure 5.11 (a) Plots of retention after heating on 100 °C for 1 hour and **(b)** log (*I*) versus (1/*kT*) plot.

However, this slight change does not affect the memory behavior of the device with a clear memory window retained throughout. Figure 5.10(e & f). show the LRS and HRS variation and it can be observed from the results that LRS is fairly stable upon heating up to 100 °C temperature, whereas a small variation in HRS is observed after 50 °C due to abrupt nature of filament rupture. The retention characteristic plot of LRS and HRS for 10^4 seconds at read voltage of 0.2 V after continuous heating of devices for 1 hour at 100 °C is shown in Figure 5.11(a). As it can be seen from the results, both LRS and HRS are stable even after 10^4 seconds. Figure 5.11(b) shows the log (*I*) versus (1/*kT*) plot for LRS and HRS. Here, *k* is the Boltzmann constant and *T* is the temperature in kelvin.The activation energy (EA) for LRS and HRS was extracted from linear fit of log (*I*) versus (1/*kT*) plot and found to be ~39 and ~163 meV, respectively. These EA values are very similar to the earlier reported values of 35 meV for LRS and 210 meV for HRS in Mo/$MoSe_2$/Ag devices with Ag as TE [Kim et al., 2019]. Higher EA values (~740 meV) have also been reported in literature for HRS in RRAM devices with different structures [Chang et al., 2015]. Lower EA values indicate lower energy requirements for state transitions.

Table 5.2: Summary of Performance Parameters of Some Recently Reported RRAM Devices with PVK and MoS_2 as an Active Material Component on Rigid and Flexible Substrates.

Switching Layer	Substrate	V_{SET} (V)	V_{RESET} (V)	I_{ON}/I_{OFF}	*Endur.*	Bending Radii. (mm)	Ret.	Ref
PBD:PVK	ITO/Glass	-1	<3.5	10^2-10^4	116	-	10^3	[Sun et al., 2015]
PVK:OXD-7	ITO/Glass	-3.1	2.3	2.5 ×10^2	60	-	10^4	[Pan et al., 2021]
MoS_2/ PVK	ITO/Glass	-3.72	4.2	70	200	-	10^4	[Fan et al., 2017]
PVK:TiO_2 NP	ITO/PET	-2	2	10^2	100	20	10^3	[Li et al., 2018]
MoS_2:rGO	ITO/PET	0.4	-0.45	10	200	10	10^4	[Wu et al., 2019]
PVK:MoS_2/ TiO_2	ITO/PEN	1.2	-1.5	~10^2	1000	7	10^4	[Saini et al., 2023]

The summary of performances of some recently reported RRAM devices with PVK and MoS_2 active material on rigid or flexible substrate is shown in Table 5.2. As it can be seen, the performance of Ag/PVK:MoS_2/TiO_2/ITO RRAM devices reported by us in this work is on higher side compared to many of these reports with low-voltage switching, high endurance, and stability suitable for exploration for flexible electronic applications.

5.4 Conclusion

High-performance flexible Ag/PVK:MoS_2/TiO_2/ITO RRAM devices were demonstrated. The novel combination of PVK:MoS_2/TiO_2 as an active layer helped the devices to show reliable resistive switching with low values of SET (1.2 V) and RESET (-1.5 V) voltages. Nonvolatile memory behavior with excellent retention more than 10000 seconds and a decent I_{ON}/I_{OFF} of over 10^2 was achieved. Ohmic conduction and SCLC mechanism in the devices were indicated by a double log I–V plot. Moreover, these devices exhibited high stability in performance upon bending and high endurance over 1000 cycles. These devices were further comprehensively investigated for their shelf life and stability for long duration. These devices were able to exhibit excellent switching behavior with a maximum V_{SET} of ~1.5 V and lowest V_{RESET} of ~-1.6 V, upon systematic characterization for memory performance for 20 months. These devices exhibited excellent shelf life, low values of and V_{SET}/V_{RESET} with high retention for more than 10^4 seconds. Moreover, the switching performance was intact upon exposure to decent humidity levels and upon heating. Although the devices exhibited almost unchanged V_{SET} and V_{RESET} values upon the variation of humidity exposure from RH of ~42% to ~99%, the magnitude of V_{SET} and V_{RESET} increased upon heating at 100 ˚C, with decay in I_{ON}/I_{OFF}. These results indicate that the proposed hybrid bilayer (PVK:MoS_2/TiO_2) can be a suitable switching layer candidate for flexible RRAM devices for realistic applications.

…